

# Composite of Magnesium and Carbonate Apatite for Biodegradable Bone Implants: A Comparative Study on Sintering and Extrusion Techniques

Iwan Setyadi <sup>a,\*</sup>, Suryadi <sup>a</sup>, I Nyoman Jujur <sup>a</sup>, Mirza Wibisono <sup>a</sup>, Damisih <sup>a</sup>, Maykel Manawan <sup>b</sup>, Krisna Adhitya <sup>a</sup>, Arif Hidayat <sup>a</sup>, Achmad Fauzi Kamal <sup>c</sup>, Rahyusalim <sup>c</sup>, Bambang Suharno <sup>d</sup>, Sugeng Supriadi <sup>e</sup>

<sup>a</sup> Research Center of Advanced Materials, National Research and Innovation Agency (BRIN), Puspiptek Area, South Tangerang, Banten, 15314, Indonesia

<sup>b</sup> Faculty of Defense Technology, Indonesia Defense University, Bogor1681, Indonesia

<sup>c</sup> Department Orthopedic and Traumatology, Faculty of Medicine, Universitas Indonesia, Cipto Mangunkusumo General Hospital, 10430, Indonesia

<sup>d</sup> Department of Metallurgical and Materials Engineering, Faculty of Engineering, Universitas Indonesia, Depok, 16424, Indonesia

<sup>e</sup> Department of Mechanical Engineering, Faculty of Engineering, Universitas Indonesia, Depok, 16424, Indonesia

Corresponding author: \*i1setyadi2810@gmail.com ; iwan015@brin.go.id

**Abstract**—Developing biodegradable bone implants using magnesium-based materials has garnered significant attention in research. Magnesium offers favorable properties, such as low density, biocompatibility, elastic modulus like bone, and high toxicity limits. However, improvements are needed in mechanical properties and degradation rate. This study focuses on enhancing these properties by developing a novel composite of magnesium with carbonate apatite (CA) reinforcement, Mg/5CA. Compared to hydroxyapatite (HA), CA offers better absorption and avoids fibrotic tissue formation. However, CA undergoes carbonate decomposition during sintering, leading to composite degradation. To address this, an extrusion process is employed to prevent carbonate decomposition. The advanced sintering and extrusion compaction processes are compared for the Mg/5CA composite, examining density, microstructure, hardness, compressive strength, and biocorrosion. Results demonstrate that extrusion increases relative density while CA slightly reduces it. Microstructural analysis reveals finer and elongated grains, tighter bonding between CA and Mg particles, and reduced microporosity in the extruded composite. Mechanical properties, including hardness distribution and compressive strength, are improved in the extruded composite, and the degradation rate decreases compared to sintering. Overall, the extrusion process effectively enhances Mg/5CA composite properties, positioning it as a promising manufacturing technique for biodegradable implant materials. This research contributes to the development of advanced biodegradable implants, which can have significant applications in the field of medical science. Further investigations in this area can contribute to the ongoing advancements in biodegradable implant technology.

**Keywords**— Biodegradable bone implant; Mg base composite material; carbonate apatite reinforcement; Mg/5CA; sintering process; extrusion process.

Manuscript received 27 Jun. 2023; revised 30 Aug. 2023; accepted 6 Nov. 2023. Date of publication 29 Feb. 2024.

IJASEIT is licensed under a Creative Commons Attribution-Share Alike 4.0 International License.



## I. INTRODUCTION

The development of magnesium-based material as supporting material for biodegradable bone implants is one of the current exciting research topics. Since no surgery is required after the implantation, it attracts various researchers [1], [2]. Magnesium has a low density, modulus close to bone, is biocompatible, and has a high toxic limit, making it attractive for biomaterial implants [1], [3]–[5]. However, to

be able to use it, Mg's mechanical properties and degradation rate must be improved [2].

One way to do this is to create a new structure in the form of a composite [2], [5]–[8]. Magnesium composite with bioceramic reinforcements, e.g., calcium phosphate-based such as Hydroxyapatite (HA), is chosen due to its biocompatibility, bioactivity, and approximate chemical composition to bone [1], [3]. Ghazizadeh developed an Mg/HA composition with HA content of 2.5 and 5%wt. [9]

while Campo has 5, 10, and 15% wt HA content. [10], [11]. They reported that the optimal characteristics were achieved in the composition of 5%wt. However, HA is difficult to absorb and tends to form a new fibrotic tissue that does not favor bone healing [12]–[15]

In this study, a powder-based magnesium composite with carbonate apatite reinforcement ( $\text{CO}_3\text{Ap}$ ;  $(\text{Ca}_{10-a}(\text{PO}_4)_6-b(\text{CO}_3)_c(\text{OH})_{2-d})$ ) was developed. Carbonate Apatite (CA) has properties like those of HA. Unlike HA, CA is more easily absorbed and does not form fibrotic tissue, so it is deemed to have more potential to help heal the bone [16]–[21].

However, the carbonate ( $\text{CO}_3^{2-}$ ) present in CA starts to decompose into  $\text{CO}_2$  gas at  $50^\circ\text{C}$ . There is a tendency to increase at  $450\text{--}650^\circ\text{C}$ , causing the product to decompose and weakening the mechanical properties [14], [16], [19], [22]. Therefore, the extrusion process is introduced to prevent carbonate decomposition [10], [11], [23], [24].

This research continues efforts to develop biodegradable Mg-xCA composites for implant materials. The initial stage has successfully made the initial solids through a warm solidification process [18], [25], [26]. Therefore, this research investigates the density, microstructure, hardness distribution, compressive strength, and biocorrosion of Mg/5CA as a result of advanced compaction using the sintering and the extrusion processes, respectively.

## II. MATERIALS AND METHODS

### A. Materials

Commercial magnesium powder (purity:  $\geq 99.9\%$ , size:  $60\text{--}300\mu\text{m}$ , Merck KGaA) and carbonate apatite (CA) powder with a size of  $\pm 74\mu\text{m}$  were used as initial raw materials. CA is a local product developed by the Research Center of Advanced Materials - BRIN.

### B. Mg/5CA Composite Preparation Process

The Mg/xCA composites made with the composition  $x = 5\%$  wt referred to the optimal composition of development in magnesium/hydroxyapatite (Mg/HA) by Campo [10], and the initial compaction process refers to previous research on the warm compacting of Mg-CA [26]. A planetary ball mill (PM400-Retsch) was used to mix Mg powder and CA powder at 200 rpm for 5 hours. The Mg-CA powder was then inserted into a mold with a 12 mm diameter. Then it was heated in a muffle furnace up to  $350^\circ\text{C}$  ( $10^\circ\text{C}/\text{minute}$  heating rate) and pressed with a pressure of 350 MPa at  $330^\circ\text{C}$  (warm compaction or WC). As a reference, pure magnesium was compacted with the same process. The Mg/xCA composites mixing process and the initial compaction stages are shown in Figure 1.



Fig. 1 Mg / 5CA powder mixing process and the initial compaction process with warm compaction (WC): (a,b) mixing process with a planetary ball mill, (c) heating process in the muffle furnace, (d) initial powder compaction process, (e) dies and punches

### C. Advance Compaction Process of Mg/5CA

The densification process after compacting was conducted with two different processes, sintering and extrusion, as

shown in Figure 2. The sintering process (Sint) was conducted in a tube furnace at  $450^\circ\text{C}$  and held for 60 minutes under a vacuum ( $P = -0.1\text{ MPa}$ ) with an oxygen content below 150 ppm [19]. The hot extrusion process (Extr) was carried out at  $350^\circ\text{C}$  with the extrusion ratio (R) of 1.44, where the initial diameter of the rod was 12 mm, and the final diameter was 10 mm.

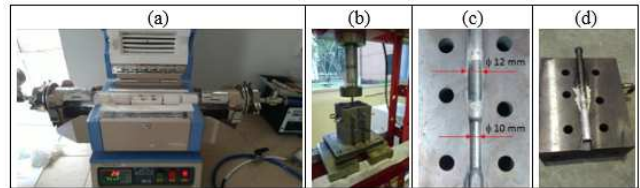


Fig. 2 Advance compaction process of Mg / 5CA: (a) sintered process, (b) extrusion process, (c) cross-section of the extrusion die, and (d) dies extrusion samples in the die.

### D. Density Testing

Density was tested using a density measuring device (DH-300X). The test was carried out at  $27^\circ\text{C}$  using Archimedes' law. The reported result was relative density, where experimental density was divided by theoretical density. The theoretical density calculation for Mg/5CA is based on the weight percentage of Mg and CA powder: 95% wt. Mg and 5% wt. CA. In this case, the density of pure Mg is  $1.73\text{ g/cm}^3$  [10], [27], [28] and the CA density is  $3.24\text{ g/cm}^3$  (developed by Research Center of Advanced Materials, BRIN).

### E. Microstructure Observation

For microstructure observation, the samples were cut in the longitudinal direction and mounted into the resin. Sandpaper with a grid size of 400 - 2000 was used for the grinding process, then polished with  $1\mu\text{m}$  alumina paste liquid. Then etched using an etching agent of 1.5 g of picric acid, 25 ml of ethanol, 5 ml of acetic acid & 10 ml of distilled water for  $\pm 20$  seconds.

Meiji Techno (Tokyo, Japan) is used to observe the microstructure of Mg/5CA. The samples were observed along its radial sections. Micro XRF Bruker-M4 Tornado (Karlsruhe, Germany) was used to observe the distribution of Ca and P as constituent elements of carbonate apatite in the magnesium matrix. Rigaku-MiniFlex 600 (Tokyo, Japan) X-ray diffraction was used to identify the Mg/5CA phase and pure Mg. The instrument was operated at 40 kV/15 mA, using  $\text{CuK}\alpha$  radiation with a scan rate of  $10^\circ/\text{min}$ , a range of  $10\text{--}90^\circ 2\theta$  and a step size of  $0.02^\circ 2\theta$ .

### F. Mechanical Properties Testing (Microhardness Testing and Compressive Strength Testing)

Stuers-DuraScan HV microhardness (Germany) was used with 9.807 N (HV1) for Mg-base. Hardness measurement starts from the direction opposite the extrusion or pressing direction, which is measured along the axial direction at 3 mm from the center. Compressive strength testing was conducted by the Universal Testing Machine (Shimadzu DT50-50-25KIT) with a sample size of  $\text{D}10 \times 12\text{ mm}$  according to the Standard of GB/T7314-2005 [29].

### G. Biocorrosion Testing

The degradation rate of Mg/5CA was determined by its corrosion rate. The corrosion rate was investigated using the potentiodynamic polarization method based on ASTM-G5-

14) [30], and the calculations refer to ASTM-G102-89 [31]. The equipment used was an electrochemical station (Zahner Zennium X and Thales XT5.0.18 software). Three electrode cells were used: a sample as a working electrode, a saturated calomel (Ag/AgCl) as a reference electrode, and platinum as a counter electrode. The test solution used was simulated body fluid (SBF) with the composition of NaCl (7,996 g), NaHCO<sub>3</sub> (0.350 g), KCl (0.224 g), K<sub>2</sub>HPO<sub>4</sub>·3H<sub>2</sub>O (0.228 g), MgCl<sub>2</sub>·6H<sub>2</sub>O (0.305 g), 1M-HCl (40 ml), then about 90% of added the total amount of HCl CaCl<sub>2</sub> (0.278 g), Na<sub>2</sub>SO<sub>4</sub> (0.071g) and (CH<sub>2</sub>OH) 3CNH<sub>2</sub> (6,057 g) [32]–[34]. The testing occurred at 37°C, pH 7.4, and a scanning rate of 5 mV/second.

### III. RESULTS AND DISCUSSION

All paragraphs must be indented. All paragraphs must be justified, i.e., both left-justified and right-justified.

#### A. Rod Samples Visual Form

The visual form of the Mg and Mg/5CA rod resulting from the advanced compaction by the sintering and hot extrusion processes is shown in Figure 3. Sintered Mg and Mg/5CA rods are 10 mm in diameter with a maximum length of 30 mm, and their shape and size are almost the same as the initial compaction (WC). Visually, both samples look neat and solid, with no burn marks, but they cannot be cut into thin shapes because they will disintegrate while cutting with a diamond cutter machine. Meanwhile, the extruded Mg and Mg-5CA rods can be made longer with a maximum length of 65 mm. It also can be cut into thin plates with a thickness of up to 1 mm.

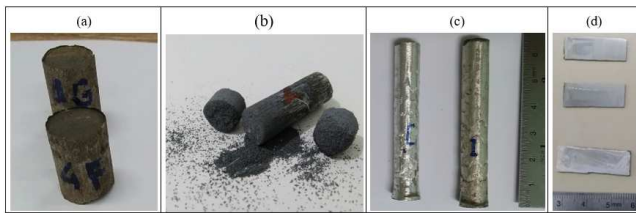


Fig. 3 Rod of pure Mg and Mg/5CA : (a) sintered samples, (b) cutting results of the sintered sample, (c) extruded samples, and (d) cutting results of the extruded sample.

#### B. Density Testing Result

The results of experimental density measurements and calculation of the relative density of Mg and Mg/5CA of the extrusion process (Extr) compared to the warm compaction process (WC), sintering process (Sint) in the previous study [19] are presented in Table 1. The relative density is calculated from the relationship between the experimental density ( $\rho_{exp.}$ ) to theoretical density ( $\rho_{theo.}$ ).

TABLE I  
THE RESULTS OF THE EXPERIMENTAL DENSITY MEASUREMENT AND THE RELATIVE DENSITY CALCULATION OF MG AND MG/5CA AS WARM COMPACTION, SINTER AND EXTRUSION

Process	Pure Mg		Mg/5CA	
	$\rho_{exp.}$ (g/cm <sup>3</sup> )	$\rho_{exp.}/\rho_{theo.}$ (%)	$\rho_{exp.}$ (g/cm <sup>3</sup> )	$\rho_{exp.}/\rho_{theo.}$ (%)
WC	1.71(2)	98.50(7) *	1.73(4)	97.64(0) *
Sint	1.72(0)	98.95(9) *	1.73(5)	97.70(4) *
Extr	1.72(6)	99.31(8)	1.74(5)	98.23(1)

Note: The theoretical density ( $\rho_{theo.}$ ) of pure Mg = 1.738 g/cm<sup>3</sup>,  $\rho_{theo.}$  of Mg/5CA=1.779 g/cm<sup>3</sup>  
\*[19]

Figure 4 shows that the relative density increases from WC, Sint, and Extr for Mg and Mg/5CA, respectively. However, adding CA causes the density of Mg/5CA to decrease compared to pure Mg. The relative density of the sintered sample (Sint) increased by 0.46% for Mg and 0.07% for Mg/5CA, while the extruded sample (Extr) sample increased by 0.8% for Mg and 0.6% for Mg/5CA compared to the initial sample (WC). This means that the extrusion process increases relative density compared to the sintering process for both Mg and Mg/5CA. In this case, the addition of CA slightly reduces the relative density increase in the Mg/5CA composite.

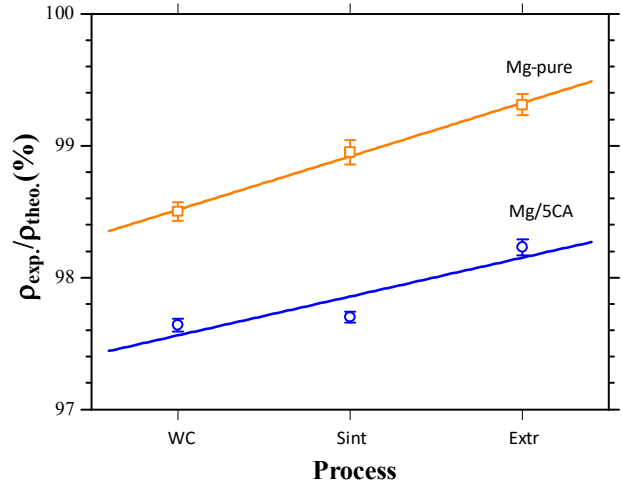


Fig. 4 Relative density curves of pure Mg and Mg/5CA as a result of the WC, Sint, and Extr processes.

#### C. The Microstructure of Samples

Figure 5 shows the microstructure of pure Mg and Mg/5CA samples after the extrusion process (Extr) compared to the warm compaction (WC) and sinter processes (Sint) in previous studies [19]. Each process is observed in the center and the edges. Pure Mg has close contact (dense) between its grain, which indicates smooth contrast between the grain and grain boundaries. In contrast, in the Mg/5CA composite, the Mg grain is encapsulated by CA, which precipitates at grain boundaries. Microporosity (black area) is also present, which reduces the relative density of the Mg/5CA composite compared to Mg.

The grain morphology for the initial (WC) and sintered (Sint) samples are relatively similar in size with equiaxed grain. However, the extruded Mg and Mg/5CA samples have a smaller grain size and elongate along the direction of the extrusion process. As reported elsewhere, the extrusion process results in strain hardening due to its deformation effect on the grains. On the other hand, the presence of CA on the grain boundaries further disrupts the dislocation where the grain boundaries act as pinning points impeding dislocation propagation. Therefore, adding CA in the extrusion process of Mg/5CA further increases the hardness of the composite.

The effect of the extrusion process starts from the edge, indicated by longer grain at the edge compared to the center. In the Mg/5CA sample, the extrusion (Extr) process is to cause the interlocking of the CA particles with the Mg particles, thus reducing microporosity, increasing relative density, and more uniform bonding between particle surfaces. This phenomenon is in line with findings from studies conducted by Guo [35] and Campo [10] on Mg/xHA.

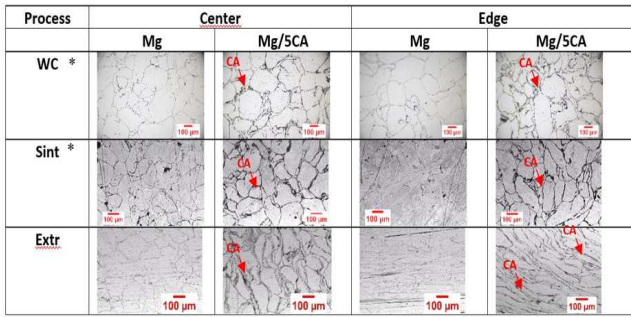


Fig. 5 Optical microscopy (OM) images of pure Mg and Mg/5CA samples after the extrusion process (Extr) compared to the warm compaction (WC) and sintering processes (Sint)

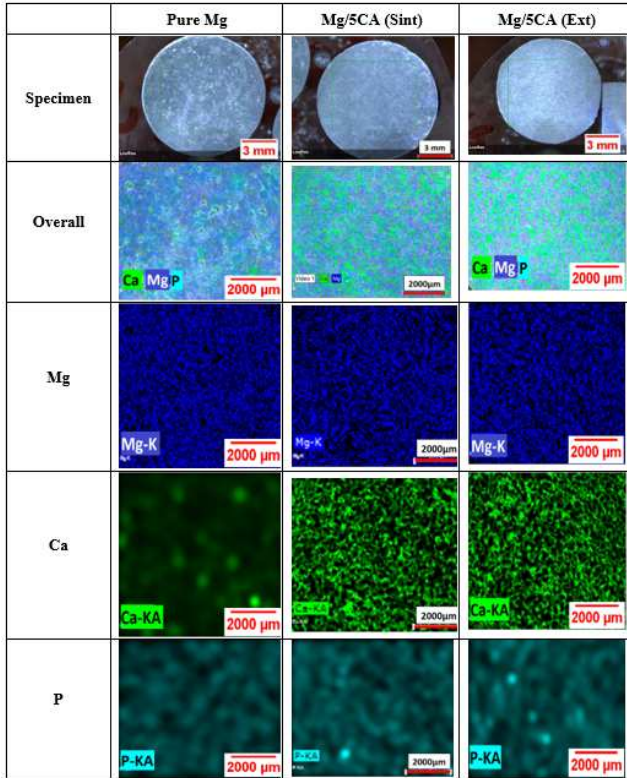


Fig. 6 Micro XRF images of pure Mg and Mg/5CA (as sintering and extrusion) showing carbonate apatite elements (Ca & P) distribution

Figure 6 shows the distribution of CA reinforcement in Mg/5CA after sintering (Sint) and extrusion (Extr) compared to pure Mg, especially the elements of Ca and P. The Ca and P contents are 1.67 wt.% and 0.92 wt.% for extruded, 1.41% and 0.77 for sintered, and Mg as the remaining elements, as shown in Table 2. This fact indicates that the operational parameters of the planetary ball mill for mixing Mg and CA powders effectively optimize the distribution of CA in the Mg matrix and minimize agglomeration.

TABLE II  
QUANTITATIVE ANALYSIS OF WT. % ELEMENTS IN MG/5CA (SINT) AND  
MG/5CA (EXT) COMPARED TO PURE MG

Element	Pure Mg (wt. %)	Mg/5CA (wt. %)	
		Sint	Extr
Mg	99.97	97.82	97.40
Ca	0.03	1.41	1.67
P	0.0	0.77	0.92

#### D. XRD Testing Result of Rod Samples

The XRD spectrum pattern of Mg/5CA in the initial process (WC), sintering (Sint) and extrusion (Extr) can be seen in Figure 7(a). The dominant peaks that appeared are 32.2, 34.4, 36.6, 47.8, 57.4, 63.1, 68.6, 69.9, 72.5, 77.8 and 81.5°, identified as Mg peaks from ICDD PDF card #00-035-0821. There are no other peaks showing other phases, such as the MgO phase, while CA peaks are not visible due to the instrument detection limit, but their appearance is obvious if observed through the micro-XRF (Figure 6).

There was a significant decrease in intensity (a.u.) in the basal slip plane (002) or in the form (hkil) = (0002) or (0001) after the sintering process and after the extrusion process. In Figure 7(b) it is also seen that there is full width half maximum (FWHM) widening of the HCP (002) slip plane, especially in the extrusion process. Grain refinement and strain hardening have occurred, increasing the compressive strength of the extruded Mg/5CA. The effect of plastic deformation on FWHM widening has also been reported in pure Ti cold-rolling processes [36]. Further details will be discussed in a separate manuscript.

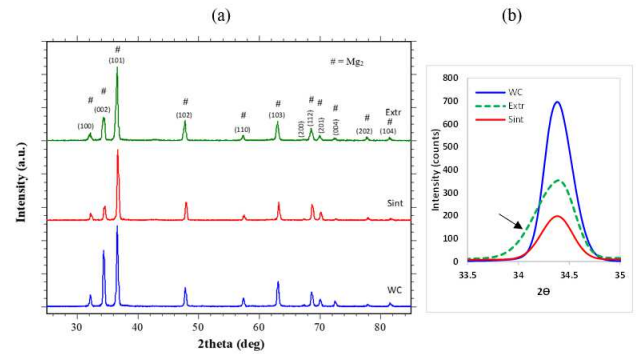
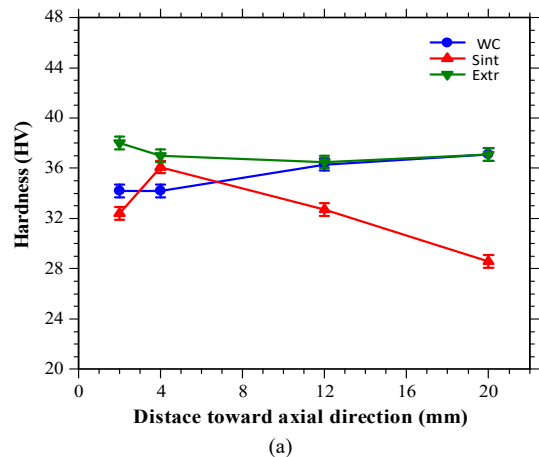


Fig. 7 (a) XRD pattern of Mg/5CA warm compaction (WC), sintering (Sint) and extrusion (Extr) processes, (b) HCP's slip plane (002) intensity and FWHM comparison

#### E. Hardness Distribution

Figure 8 shows the hardness distribution curves for pure Mg and Mg/5CA rods, respectively (as a result of WC, Sint, and Extr.). Advanced compaction and CA content affect the hardness distribution of magnesium composites. Extruded Mg and Mg/5CA rods (Extr) have a relatively uniform hardness distribution, but not for sintered rods (Sint) and initial compaction (WC), it tends to decrease in the opposite direction of pressing.



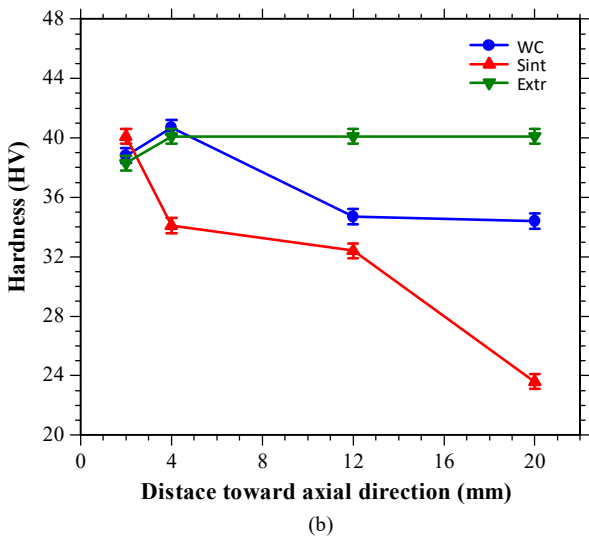


Fig. 8 Hardness distribution curves of (a) pure Mg and (b) Mg/5CA rods

The presence of CA in the extruded Mg/5CA composite increases the overall value of the hardness distribution compared to the extruded Mg. However, the sintered Mg/5CA shows a significant decrease in the hardness distribution. The highest reduction in hardness distribution is 17% at the measuring point of 20 mm from the initial pressing. In the sintered Mg/5CA, the sintering process is conducted at a temperature of 450°C. At a temperature of 450°C, carbonate ( $\text{CO}_3^{2-}$ ) in CA can decompose into  $\text{CO}_2$  gas. This gas is thought to be trapped and form microporosity, so that it can weaken the binding strength of Mg/xCA [19], [37]. On the other hand, the morphology of the sintered grains is still in the form of equilibrium, relatively the same as the initial compaction (WC) conditions, and there is no strain hardening. The rod is shorter, depending on how length the WC rod can be produced.

The uniformity of the distribution of hardness occurs because of bond strengthening resulting from the extrusion process. The extrusion process makes the grains elongate and smaller, which causes strain hardening. Furthermore, in extruded Mg/5CA composites, Mg and CA particles are interlocked, making the bonds between the particles denser and reducing microporosity. Therefore, the rods are longer and can be sliced into plates up to 1 mm thick. The obtained hardness ranges of along rod respectively are 39.3-40.1 Hv (Extr), 23.6-40.1 Hv (Sint), 34.4-39.3 Hv (WC) for Mg/5CA and 36.5-38 Hv (Extr), 28.6-36.1 Hv (Sint), 34.2-37.1 Hv (WC) for Mg.

#### F. Compressive Strength

Compressive strength curves of Mg/5CA rods as Warm Compaction (WC), Sintered (Sint) and Extruded (Extr) are shown in Fig. 9. The compressive strength of Mg/5CA after extrusion is the best compared to that after sintering. The increase after extrusion was 61% (after extrusion), but after sintering there was a decrease of 39% compared to the initial conditions as warm compaction (WC). In this case the compressive strength of Mg/5CA as WC is 67.1 MPa.

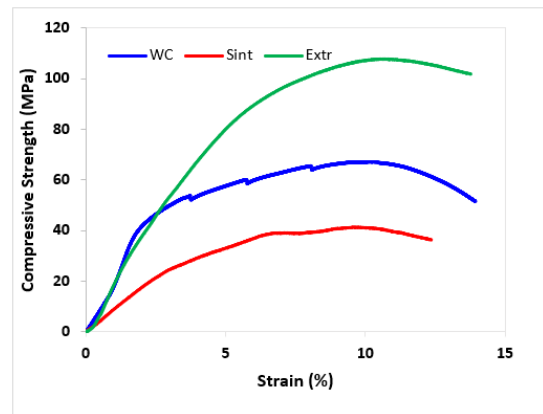


Fig. 9 Compressive strength

Like the description of the hardness distribution, the extrusion process makes the grains elongated and smaller, causing the Mg and CA particles to interlock, the bonds between the particles to be denser, and the microporosity to be reduced. This phenomenon has been reported in other deformation processes. Thickness reduction in the post-rolling annealing process increases the bond strength of the ceramic/metal matrix (Al/SiC-Gr) particles, as reported by Reihanian [38]. Grain deformation causes interlocking between Mg-CA, it is needed for further observation of the interface between Mg dan CA contributed to the strengthening of these composites. An increase in compressive strength with this extrusion process has also been reported in Campo's study [10] compared to the Mg/5HA microwave sintering process reported by Xiong [29]. The increase in the compressive strength of Mg/5CA extrusion is also shown by the widening FWHM compared to the sintering process, as shown in Figure 7(b). The decrease in compressive strength after sintering is believed to be due to pyrolysis, where  $\text{CO}_3^{2-}$  is decomposed into  $\text{CO}_2$  gas which can form microporosity [19], [29]. Besides that, the grain shape is still equiaxed, so there is no interlocking between Mg-CA grains due to grain deformation.

#### G. Biocorrosion Test Results

Figure 10 shows the potentiodynamic polarization curve and the corrosion rate (CR) comparison graph of pure Mg and Mg/5CA. Advance compaction and CA content affect the corrosion rate of magnesium composites. The extrusion process (Extr) causes a decrease in the corrosion rate compared to the sintering process (Sint) and the initial compaction process (WC) for pure Mg and Mg/5CA. The extrusion process expands the interlocking area of Mg and CA particles, making them denser and believed to have less porosity than the sintering process. As has been reported in a previous study, sintered Mg/5CA has equiaxed grains shape, almost the same as WC grains. In addition, the possibility of microporosity in Mg/5CA still exists due to the pyrolysis effect of  $\text{CO}_3^{2-}$  to  $\text{CO}_2$  gas [18], [19], [37], so the density is not optimal.

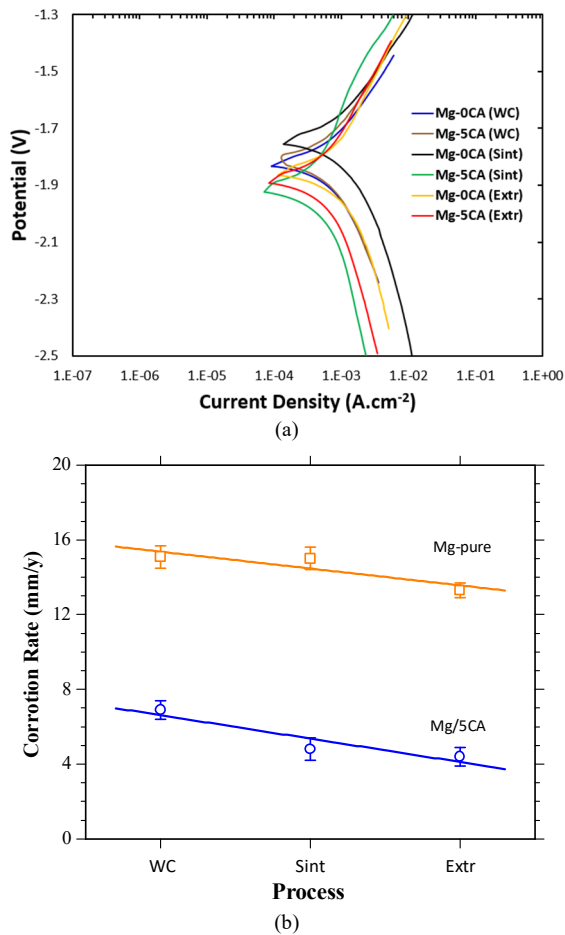


Fig. 10 (a) Potentiodynamic polarization curve and (b) Corrosion rate (CR) comparison graph of pure Mg and Mg/5CA

Besides that, there are reports that the smaller the grains, the more grain boundary defects that occur, so the faster the oxide layer (MgO) and the passive layer of Mg(OH)<sub>2</sub> are formed on the surface of Mg and inhibit the corrosion rate [39], [40]. This factor causes the corrosion resistance of extruded Mg/5CA and pure Mg to be better than that of sintered ones.

Meanwhile, adding CA also significantly decreased the corrosion rate of Mg/5CA compared to pure Mg. There are reports that the Mg(OH)<sub>2</sub> layer has high permeability and is unstable, especially in NaCl solution [41]–[44]. Acid ions in SBF, such as PO<sub>4</sub><sup>3-</sup>, CO<sub>3</sub><sup>2-</sup>, and Cl<sup>-</sup> also continuously absorb the passive layer of Mg(OH)<sub>2</sub> and form MgCl<sub>2</sub>, which is water soluble. This condition accelerates corrosion again. With the addition of HA (hydroxyapatite) in Mg-based composites, the acid ions will be absorbed and then form Ca-P deposits as a new protective layer so that the corrosion rate drops again [8], [9], [45]–[47]. Because the constituent elements of CA are almost the same as HA, this pattern of decreasing corrosion rate is believed to also occur in the Mg/5CA composite.

In Figure 10 (b), it can be seen that the decrease in corrosion rate due to advanced compaction is 12% (as extrusion), 0.7% (as sintering) for pure Mg, and 36% (as extrusion), 30% (as sintering) for Mg/5CA compared to the initial compaction results (WC). Meanwhile, the largest percentage of corrosion rate reduction due to the addition of CA is 67% in the extruded Mg/5CA compared to the extruded

pure Mg. The lowest corrosion rate is obtained at extruded Mg/5CA (4.4 mm/y), followed by sintered results (4.8 mm/y) and WC results (6.9 mm/y).

#### IV. CONCLUSION

Efforts have been made to develop powder-based Mg/5CA composites through an advanced compaction process with sintering and extrusion processes. The extrusion process makes the grains smaller and elongated due to a reduction in Mg and Mg/5CA rods. Extruded rods are denser, have a uniform hardness distribution and higher compaction strength, and are longer than sintered rods, so they can be sliced into plates up to 1mm thick. No other phases, such as MgO are found. CA reinforcement particles are also seen to be more evenly distributed in the Mg/5CA composite. The addition of CA and the extrusion process can significantly increase corrosion resistance compared to pure magnesium with the same process.

The sintering process has not uniformly distributed the density of Mg/5CA rods. The grain morphology is relatively the same as the initial compaction (WC), so it tends to crumble when sliced. The sintering temperature causes carbonate pyrolysis (CO<sub>3</sub><sup>2-</sup>) in CA, so the micropores formed by the trapped CO<sub>2</sub> gas are potential factors that cause a decrease in the density and the hardness distribution. Therefore, a combination of warm compaction and extrusion can be recommended as part of the fabrication process in developing Mg/5CA for biodegradable implant material.

#### NOMENCLATURE

CA	carbonate-apatite (Ca <sub>10-a</sub> (PO <sub>4</sub> ) <sub>6-b</sub> (CO <sub>3</sub> ) <sub>c</sub> (OH) <sub>2-d</sub> )
Mg/5CA	Magnesium-based composite used 5% wt. carbonate-apatite
WC	warm compaction
Sint	sintering
Extr	extrusion

#### Subscripts

ρ <sub>exp</sub>	experimental density
ρ <sub>theo</sub>	theoretical density

#### ACKNOWLEDGMENT

The authors thank the Research Center for Advanced Materials - National Research and Innovation Agency (BRIN) for facilitating this research. Thanks are also conveyed to all parties in facilitating this research, especially the Department of Metallurgical and Materials Engineering and the Department of Mechanical Engineering, Faculty of Engineering, University of Indonesia.

#### REFERENCES

- [1] Z. Shan, X. Xie, X. Wu, S. Zhuang, and C. Zhang, "Development of degradable magnesium-based metal implants and their function in promoting bone metabolism (A review)," *J. Orthop. Transl.*, vol. 36, no. July, pp. 184–193, 2022, doi:10.1016/j.jot.2022.09.013.
- [2] L. D. C. Gutiérrez Púa, J. C. Rincón Montenegro, A. M. Fonseca Reyes, H. Zambrano Rodríguez, and V. N. Paredes Méndez, "Biomaterials for orthopedic applications and techniques to improve corrosion resistance and mechanical properties for magnesium alloy: a review," *J. Mater. Sci.*, vol. 58, no. 9, pp. 3879–3908, 2023, doi:10.1007/s10853-023-08237-5.

- [3] M. Rahman, N. K. Dutta, and N. Roy Choudhury, "Magnesium Alloys With Tunable Interfaces as Bone Implant Materials," *Front. Bioeng. Biotechnol.*, vol. 8, no. June, 2020, doi: 10.3389/fbioe.2020.00564.
- [4] M. R. Sahu, T. S. S. Kumar, and U. Chakkingal, "A review on recent advancements in biodegradable Mg-Ca alloys," *J. Magnes. Alloy.*, vol. 10, no. 8, pp. 2094–2117, 2022, doi: 10.1016/j.jma.2022.08.002.
- [5] F. Khorashadizade *et al.*, "Overview of magnesium-ceramic composites: mechanical, corrosion and biological properties," *J. Mater. Res. Technol.*, vol. 15, pp. 6034–6066, 2021, doi:10.1016/j.jmrt.2021.10.141.
- [6] K. N. Braszczynska-Malik, "Types of component interfaces in metal matrix composites on the example of magnesium matrix composites," *Materials (Basel)*, vol. 14, no. 18, 2021, doi: 10.3390/ma14185182.
- [7] J. Su, J. Teng, Z. Xu, and Y. Li, "Biodegradable magnesium-matrix composites: A review," vol. 27, no. 6, pp. 724–744, 2020.
- [8] M. Khodaei, F. Nejatidanesh, M. J. Shirani, S. Iyengar, H. Sina, and O. Savabi, "Magnesium/Nano-hydroxyapatite Composite for Bone Reconstruction: The Effect of Processing Method," *J. Bionic Eng.*, vol. 17, no. 1, pp. 92–99, 2020, doi: 10.1007/s42235-020-0007-6.
- [9] E. Ghazizadeh, A. H. Jabbari, and M. Sedighi, "In vitro corrosion-fatigue behavior of biodegradable Mg/HA composite in simulated body fluid," *J. Magnes. Alloy.*, vol. 9, no. 6, pp. 2169–2184, 2021, doi:10.1016/j.jma.2021.03.027.
- [10] R. del Campo, B. Savoini, A. Muñoz, M. A. Monge, and G. Garcés, "Mechanical properties and corrosion behavior of Mg-HAP composites," *J. Mech. Behav. Biomed. Mater.*, vol. 39, pp. 238–246, 2014, doi: 10.1016/j.jmbbm.2014.07.014.
- [11] R. del Campo, B. Savoini, A. Muñoz, M. A. Monge, and R. Pareja, "Processing and mechanical characteristics of magnesium-hydroxyapatite metal matrix biocomposites," *J. Mech. Behav. Biomed. Mater.*, vol. 69, no. November 2016, pp. 135–143, 2017, doi:10.1016/j.jmbbm.2016.12.023.
- [12] K. Kudoh *et al.*, "Reconstruction of rabbit mandibular bone defects using carbonate apatite honeycomb blocks with an interconnected porous structure," *J. Mater. Sci. Mater. Med.*, vol. 34, no. 1, 2023, doi:10.1007/s10856-022-06710-2.
- [13] Y. S. Shin, M. K. Jo, Y. S. Cho, and S. H. Yang, "Diffusion-Controlled Crystallization of Calcium Phosphate in a Hydrogel toward a Homogeneous Octacalcium Phosphate/Agarose Composite," *ACS Omega*, vol. 7, no. 1, pp. 1173–1185, 2022, doi:10.1021/acsomega.1c05761.
- [14] L. H. Thang, L. T. Bang, B. D. Long, N. A. Son, and S. Ramesh, "Effect of Carbonate Contents on the Thermal Stability and Mechanical Properties of Carbonated Apatite Artificial Bone Substitute," *J. Mater. Eng. Perform.*, vol. 32, no. 3, pp. 1006–1016, 2023, doi: 10.1007/s11665-022-07169-6.
- [15] M. Du, J. Chen, K. Liu, H. Xing, and C. Song, "Recent advances in biomedical engineering of nano-hydroxyapatite including dentistry, cancer treatment and bone repair," *Compos. Part B Eng.*, vol. 215, no. February, p. 108790, 2021, doi: 10.1016/j.compositesb.2021.108790.
- [16] K. Ishikawa and K. Hayashi, "Carbonate apatite artificial bone," *Sci. Technol. Adv. Mater.*, vol. 22, no. 1, pp. 683–694, 2021, doi:10.1080/14686996.2021.1947120.
- [17] K. Ishikawa, "Carbonate apatite bone replacement: Learn from the bone," *J. Ceram. Soc. Japan*, vol. 127, no. 9, pp. 595–601, 2019, doi:10.2109/jcersj2.19042.
- [18] I. Setyadi *et al.*, "Characteristics investigation of the initial development of miniplate made from composite of magnesium/carbonate apatite fabricated by powder metallurgy method for biodegradable implant applications," in *Key Engineering Materials*, Trans Tech Publications Ltd, 2020, pp. 194–198, doi:10.4028/www.scientific.net/KEM.833.194.
- [19] I. Setyadi *et al.*, "Fabrication of Magnesium-Carbonate Apatite by Conventional Sintering and Spark Plasma Sintering for Orthopedic Implant Applications," *Sains Malaysiana*, vol. 51, no. 3, pp. 883–894, 2022, doi: 10.17576/jsm-2022-5103-22.
- [20] Y. K. Eriwati, D. Arsista, S. Triaminingsih, and Sunarso, "Effect of CaSO<sub>4</sub> dissolution-precipitation time on formation of porous carbonate apatite as bone replacement material," *J. Biomimetics, Biomater. Biomed. Eng.*, vol. 44, pp. 83–90, 2020, doi:10.4028/www.scientific.net/JBBBE.44.83.
- [21] K. Hayashi, M. L. Munar, and K. Ishikawa, "Effects of macropore size in carbonate apatite honeycomb scaffolds on bone regeneration," *Mater. Sci. Eng. C*, vol. 111, no. February, p. 110848, 2020, doi:10.1016/j.msec.2020.110848.
- [22] C. H. Yoder, K. R. Stepien, and T. M. Edner, "A new model for the rationalization of the thermal behavior of carbonated apatites," *J. Therm. Anal. Calorim.*, vol. 140, no. 5, pp. 2179–2184, 2020, doi:10.1007/s10973-019-08946-7.
- [23] A. J. Rahyussalim *et al.*, "Synthesis, Structural Characterization, Degradation Rate, and Biocompatibility of Magnesium-Carbonate Apatite (Mg-Co<sub>3</sub>Ap) Composite and Its Potential as Biodegradable Orthopaedic Implant Base Material," *J. Nanomater.*, vol. 2021, 2021, doi: 10.1155/2021/6615614.
- [24] X. Wang, X. Wang, X. Hu, and K. Wu, "Effects of hot extrusion on microstructure and mechanical properties of Mg matrix composite reinforced with deformable TC4 particles," *J. Magnes. Alloy.*, vol. 8, no. 2, pp. 421–430, 2020, doi: 10.1016/j.jma.2019.05.015.
- [25] A. J. Rahyussalim, S. Supriadi, A. F. Kamal, A. F. Marsetio, and P. M. Pribadi, "Magnesium-carbonate apatite metal composite: Potential biodegradable material for orthopaedic implant," in *AIP Conference Proceedings*, AIP Publishing LLC, 2019, p. 02021, doi:10.1063/1.5096689.
- [26] I. Setyadi, A. F. Marsetio, A. F. Kamal, A. J. Rahyussalim, S. Supriadi, and B. Suharno, "Microstructure and microhardness of carbonate apatite particle-reinforced Mg composite consolidated by warm compaction for biodegradable implant application," *Mater. Res. Express*, 2020, doi: 10.1088/2053-1591/ab7d70.
- [27] M. M. Jamel, M. M. Jamel, and H. F. Lopez, "Designing Advanced Biomedical Biodegradable Mg Alloys: A Review," *Metals (Basel)*, vol. 12, no. 1, pp. 1–15, 2022, doi: 10.3390/met12010085.
- [28] M. Pizzi, F. De Gaetano, M. Ferroni, F. Boschetti, and M. Annoni, "A Deep-Hole Microdrilling Study of Pure Magnesium for Biomedical Applications," *Micromachines*, vol. 14, no. 1, pp. 1–16, 2023, doi:10.3390/mi14010132.
- [29] G. Xiong *et al.*, "Characterization of biomedical hydroxyapatite/magnesium composites prepared by powder metallurgy assisted with microwave sintering," *Curr. Appl. Phys.*, vol. 16, no. 8, pp. 830–836, 2016, doi: 10.1016/j.cap.2016.05.004.
- [30] ASTM, "ASTM-G5-14," 2021.
- [31] ASTM, "ASTM-G102-89," 2019.
- [32] T. Kokubo, H. Kushitani, S. Sakka, T. Kitsugi, and T. Yamamuro, "Solutions able to reproduce in vivo surface-structure changes in bioactive glass-ceramic A-W3," *J. Biomed. Mater. Res.*, vol. 24, no. 6, pp. 721–734, 1990, doi: 10.1002/jbm.820240607.
- [33] J. Čović, I. Jovanović, A. Zarubica, A. Bojić, and M. Randelović, "Morpho-Structural Characterization and Electrophoretic Deposition of Xonotlite Obtained by a Hydrothermal Method," *Iran. J. Chem. Chem. Eng.*, vol. 41, no. 6, pp. 1932–1941, 2022, doi:10.30492/ijcce.2021.131277.4241.
- [34] B. A. Witika, J. C. Stander, V. J. Smith, and R. B. Walker, "Nano co-crystal embedded stimuli-responsive hydrogels: A potential approach to treat HIV/AIDS," *Pharmaceutics*, vol. 13, no. 2, pp. 1–21, 2021, doi: 10.3390/pharmaceutics13020127.
- [35] Y. Guo *et al.*, "The microstructure, mechanical properties, corrosion performance and biocompatibility of hydroxyapatite reinforced ZK61 magnesium-matrix biological composite," *J. Mech. Behav. Biomed. Mater.*, vol. 123, no. May, p. 104759, 2021, doi:10.1016/j.jmbbm.2021.104759.
- [36] C. Gurau, G. Gurau, V. Mitran, A. Dan, and A. Cimpean, "The influence of severe plastic deformation on microstructure and in vitro biocompatibility of the new Ti-Nb-Zr-Ta-Fe-O alloy composition," *Materials (Basel)*, vol. 13, no. 21, pp. 1–15, 2020, doi:10.3390/ma13214853.
- [37] Y. Doi *et al.*, "Pyrolysis–gas chromatography of carbonate apatites used for sintering," *J. Biomed. Mater. Res.*, vol. 29, no. 11, pp. 1451–1457, 1995, doi: 10.1002/jbm.820291117.
- [38] M. Reihanian, A. Baharloo, and S. M. Lari Baghal, "Wear-Resistant Al/SiC-Gr Hybrid Metal Matrix Composite Fabricated by Multiple Annealing and Roll Bonding," *J. Mater. Eng. Perform.*, vol. 27, no. 12, pp. 6676–6689, 2018, doi: 10.1007/s11665-018-3740-9.
- [39] E. Gerashi, R. Alizadeh, and T. G. Langdon, "Effect of crystallographic texture and twinning on the corrosion behavior of Mg alloys: A review," *J. Magnes. Alloy.*, vol. 10, no. 2, pp. 313–325, 2022, doi: 10.1016/j.jma.2021.09.009.
- [40] A. Bahmani, S. Arthanari, and K. S. Shin, "Formulation of corrosion rate of magnesium alloys using microstructural parameters," *J. Magnes. Alloy.*, vol. 8, no. 1, pp. 134–149, 2020, doi:10.1016/j.jma.2019.12.001.
- [41] K. Sarayama *et al.*, "Corrosion Properties of the  $\beta$ -Mg17Al12 Phase in NaCl Solutions," *Mater. Trans.*, vol. 63, no. 6, pp. 911–917, 2022, doi:10.2320/matertrans.MT-MA2022023.
- [42] L. Wei and Z. Gao, "Recent research advances on corrosion mechanism and protection, and novel coating materials of magnesium

- alloys: a review,” *RSC Adv.*, vol. 13, no. 12, pp. 8427–8463, 2023, doi:10.1039/d2ra07829e.
- [43] L. Xu, X. Liu, K. Sun, R. Fu, and G. Wang, “Corrosion Behavior in Magnesium-Based Alloys for Biomedical Applications,” *Materials (Basel)*, vol. 15, no. 7, 2022, doi: 10.3390/ma15072613.
- [44] P. Das, T. S. S. Kumar, K. K. Sahu, and S. Gollapudi, “Corrosion, stress corrosion cracking and corrosion fatigue behavior of magnesium alloy bioimplants,” *Corros. Rev.*, vol. 40, no. 4, pp. 289–333, 2022, doi: 10.1515/corrrev-2021-0088.
- [45] I. Nakahata, Y. Tsutsumi, and E. Kobayashi, “Mechanical Properties and Corrosion Resistance of Magnesium – Hydroxyapatite Composites Fabricated,” *Metals (Basel)*, vol. 10, no. 1314, pp. 1–14, 2020.
- [46] A. S. Gnedkov *et al.*, “The detailed corrosion performance of bioresorbable Mg-0.8Ca alloy in physiological solutions,” *J. Magnes. Alloy.*, vol. 10, no. 5, pp. 1326–1350, 2022, doi:10.1016/j.jma.2021.11.027.
- [47] R. Radha and D. Sreekanth, “Mechanical and corrosion behaviour of hydroxyapatite reinforced Mg-Sn alloy composite by squeeze casting for biomedical applications,” *J. Magnes. Alloy.*, vol. 8, no. 2, pp. 452–460, 2020, doi: 10.1016/j.jma.2019.05.010.